Dispersion of Tracers by Ocean Gyres

K. J. RICHARDS

Department of Oceanography, University of Southampton, Highfield, Southampton, United Kingdom

Y. JIA

Institute of Oceanographic Sciences, Rennell Centre, Chilworth, Southampton, United Kingdom

C. F. ROGERS

B.P. Research, Sunbury-upon-Thames, United Kingdom

(Manuscript received 29 December 1993, in final form 5 August 1994)

ABSTRACT

The dispersion of a tracer by a two-dimensional gyre circulation is studied using simple numerical models. Two approaches are taken: a random walk model formulated in a streamline coordinate system and the numerical solution of the advection–diffusion equation. A number of different gyres are considered. Attention is focused on the characteristics of the gyre that determine the spreading and mixing time of the tracer. The authors find that the dispersion by a given gyre can be characterized in terms of a bulk Péclet number and the three length scales: L the horizontal width of the gyre, l the width of the boundary current, and $\mathcal{L}$ the length of the boundary current. By taking into account the length of the boundary layer, gyre dispersion is found to conform moderately well with previous analytic models, in particular the partitioning between weak and strong diffusive regimes, even though the shear characteristics may be quite variable across the gyre. The analytic models become less valid as the length of the boundary layer increases. Simple expressions are given for the cross-streamline diffusion coefficient and mixing time in terms of the characteristics of the gyre. An important conclusion coming from the present study is the importance of the structure of the recirculation region in determining the shape of the tracer distribution. The results highlight the need for care in comparing model tracer fields with observed tracer distributions.

1. Introduction

Tracer fields in the ocean contain information about the ocean circulation. How much useful information and how best to extract this information are still questions with unknown answers. Two types of investigation exist. The direct approach is one in which a model for the dispersion of a given tracer with a given circulation pattern is integrated in time and the results compared with observations. A best "fit" to observations of the tracer in the ocean is then made by "tuning" the model circulation parameters [studies include the "pipeline" model of Jenkins (1988) and the 2D modeling of Sarmiento et al. (1990)]. In contrast inverse techniques start from the observed tracer field and attempt to provide the "best" flow field consistent with the observations and dynamical constraints (e.g., Wunsch 1988).

Although the inverse method is attractive it often presupposes no prior knowledge of how a given circulation field will disperse a given tracer and what characteristics of the gyre circulation the tracer distribution is sensitive to. To take an extreme example, with no dynamical constraints there are an infinite number of solutions involving varying ratios of advection and diffusion for any given tracer field. The approach taken here is a direct one and is aimed at developing an understanding of the factors that influence tracer distributions and the rate at which they may be spread over an ocean gyre. As we will find, the dispersion of a tracer is very dependent on the shape of the gyre, suggesting that the horizontal shear in a given system will place strong constraints on inverse solutions.

A number of recent studies have used the direct approach to give estimates of the Péclet number of the ocean (the ratio of diffusion to advection timescales) and the effect of mixing on the apparent "age" of a tracer. These include Sarmiento et al. (1990), Theile and Sarmiento (1990), Musgrave (1990), and Warner (1988). What these authors have failed to establish is the effect of the assumed circulation on their conclu-

Corresponding author address: Dr. K. J. Richards, Department of Oceanography, University of Southampton, Highfield, Southampton SO17 1BJ, United Kingdom.
E-mail: kelvin@ocean.soton.ac.uk

sions. The Stommel gyre has figured strongly in previous studies. We need to know the sensitivity of results to the gyre shape.

As a starting point, in this paper we consider the dispersion of a tracer cloud released in a two-dimensional recirculating flow. We employ both random walk models and the advection–diffusion equation to study the dispersion of the cloud in a variety of gyre shapes. Two works that have been influential in our understanding of tracer dispersion by gyres are Rhines and Young (1983) and Young (1984) (referred to here as RY and Y, respectively). They give analytic results for the rate of mixing both along and across streamlines. In addition, Y shows how the western boundary current of a gyre can reduce the mixing time of the gyre much below the diffusive timescale by bringing streamlines close together. He was led to distinguish two regimes in terms of the width of the boundary layer, both valid for asymptotically large Péclet number. In the weak diffusive regime, with a relatively wide boundary layer, the tracer is quickly mixed along streamlines with a subsequent slower diffusion across streamlines to achieve a uniformly mixed state. In the strong diffusive regime, with a narrow boundary layer, the across streamline diffusion is sufficiently great to mix tracer across all streamlines in one or two passes through the boundary current. The applicability of these asymptotic regimes and the mixing rates need to be tested, particularly in a gyre in which the shear characteristics may vary greatly across the gyre.

A significant part of the analysis reported here is done in a streamline coordinate framework. Such a framework helps in the interpretation of the results. An important result coming from the present work is the sensitivity of the gyral mixing on the shear in the recirculation region of the gyre, different gyres giving different mixing rates and tracer dispersion. We suggest and test simple expressions for the cross-streamline diffusion coefficient and mixing time in terms of the characteristics of the gyre.

Although the present study is restricted to steady gyres with a constant diffusion coefficient, this does allow a thorough examination of the system. The analysis should be helpful in the interpretation of more complex systems. A study of transient tracers with source/sink distributions will be reported in a later paper.

2. Random walk models

The technique of studying dispersion processes using random walk models is a well-tried technique [see Allen (1982) for a geophysical example]. A large, but finite, number of particles is released into a known mean flow field. Diffusion is modeled by making the particles undergo a displacement of given length but random orientation at discrete time intervals. Usually the advection of particles by the mean velocity field is done by a simple forward extrapolation in time on a Cartesian grid. For a recirculating gyre this has a fundamental drawback. The extrapolation is continually pushing particles off the curved streamlines and causing an outward migration of particles. To achieve moderate accuracy requires very small time steps and undermines the otherwise efficient random walk model.

To overcome the problem of particles not tracking the mean streamline in the absence of diffusion we choose to use a streamline coordinate system (Fig. 1). In terms of polar coordinates (r, θ) the streamline can be defined as

$$\psi = g(r, \theta) \tag{1}$$

with the associated inverse function

$$r = f(\psi, \theta). \tag{2}$$

Equating ψ with the streamfunction, the particle position is given by the value of the streamfunction (which for a given particle is constant for a flow with no diffusion) and its position on the streamline given here by θ. The rate of change of position along the streamline is given by

$$\frac{\partial \theta}{\partial t} = \frac{1}{r}\frac{\partial \psi}{\partial r}. \tag{3}$$

For a gyre specified by $\psi = g(r, \theta)$ particles can be advected around the gyre using a finite-difference version of (3) with the particles remaining on a streamline regardless of the size of the time step. Note that using this system the streamline cannot be so convoluted that f becomes a multivalued function. A more general measure of position along the streamline is introduced in section 2b.

At time intervals of Δt the particle undergoes a random walk. To ensure uniform diffusion this is done in (r, θ) space. The step has a given displacement length Δr in a random direction θ'. The equiv-

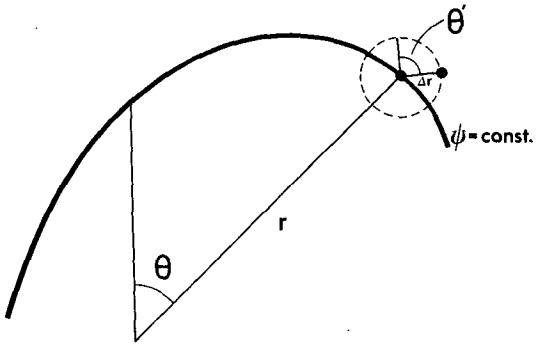

FIG. 1. Streamline coordinate system (ψ, θ) defined in terms of the polar coordinates (r, θ). The random jump from the streamline is defined by $(\Delta r, \theta')$.

alent diffusion coefficient, summing over many particles, is then

$$\kappa = \frac{\Delta r^2}{2\Delta t}.$$

Advecting by the mean flow in (ψ, θ) space and diffusing in (r, θ) space requires the position of particles to be mapped between the two spaces. We therefore need to specify both mappings (1) and (2).

We have chosen to work in polar coordinates because useful model gyres can be constructed (section 2a). The model can be equally well formulated using a streamfunction that is specified in Cartesian coordinates (x, y) such as the Stommel gyre considered in section 2b. However, as is the case for the Stommel gyre, the inverse mapping $(x, y) \rightarrow (\psi, \theta)$ will in general have to be constructed numerically.

a. *Model gyres*

A useful start is to consider the streamfunction

$$\psi = -\frac{e^{rh(\theta)} - 1}{h(\theta)}, \tag{4}$$

which has the inverse

$$r = \frac{1}{h(\theta)} \ln(1 - \psi h(\theta)). \tag{5}$$

The velocity component along the streamline u_θ is then

$$u_\theta = -e^{rh(\theta)}. \tag{6}$$

The function $h(\theta)$ controls the non-axisymmetric nature of the gyre. For $h(\theta) = 0$, the gyre is axisymmetric with $\psi = r$ and $u_\theta = 1$. We choose

$$h(\theta) = A \cos^{2n}\frac{\theta}{2}. \tag{7}$$

We shall denote this gyre, specified by (4) and (7), as Gyre 1. Note that the velocity and length scales have been normalized such that $|u_\theta| = 1$ at $(r, \theta) = (1, \pi)$. The Péclet number is then simply the inverse of the diffusion coefficient; namely, $\text{Pe} = 2\Delta t/\Delta r^2$.

The gyre with $A = 6$ and $n = 8$ is shown in Fig. 2. The gyre has a characteristic shape not unlike that of a wind-driven anticyclonic ocean gyre. The flow to the right (east) of center ($\theta = \pi$) is uniform (southward) with distance from the center. The flow to the left (west) ($\theta = 0$) is concentrated in a narrow current, equivalent to a western boundary current. The advantage of the model gyre is that the strength of the return flow (increasing A narrows and strengthens the flow) and the extent of the intense flow (decreasing n increases the proportion of the flow which is intensified) can be varied independently. (Using the analogy with an ocean gyre, increasing A narrows the boundary current while decreasing n increases the length of the boundary current). To relate the results of this simple gyre to those of more physical gyres we shall refer to the intense region of flow as the "boundary current," although there is no physical boundary in the model, with the rest of the gyre referred to as the "recirculation region." Since there is no boundary in the model we shall restrict the study to flows with high Péclet number to avoid an excessive spread of the particle cloud across many streamlines. The effect of a boundary and low Péclet numbers will be considered with later gyres.

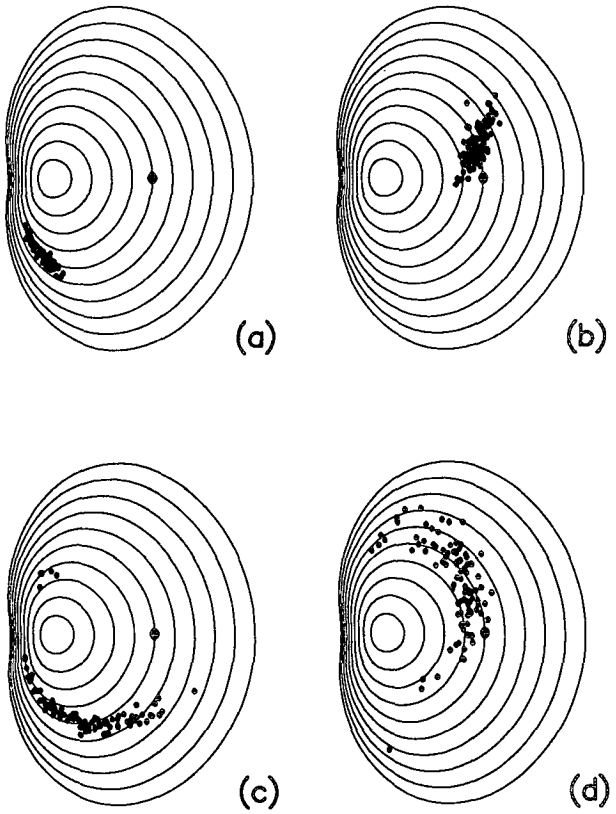

FIG. 2. Dispersion of a cloud of particles in Gyre 1 ($A = 6$, $n = 8$) released at $(1, \pi)$ at time increments of $\pi/2$; Pe = 500 (only 200 particles shown). The coordinate system is such that $r = 0$ is at the center of the gyre and $\theta = 0$ is a line starting at the center of the gyre and directed to the left (west).

The circulation time of the gyre, T_c, is a function of ψ. With $A = 0$ the circulation time increases linearly with ψ. On $\psi = 1$, $T_c = 2\pi$. Increasing A decreases the circulation time for a given streamline. With $A = 6$ and $n = 8$, T_c is reduced to 3.5 on $\psi = 1$. The variation of T_c with ψ, however, remains approximately linear.

Figure 2 shows the dispersion of a group of particles released at $(r, \theta) = (1, \pi)$ with the Péclet number Pe = 500. After the first passage through the boundary current (Fig. 2b) the particles have been dispersed across a number of streamlines but with little spread along streamlines. During the subsequent recirculation,

where $\partial\theta/\partial t \sim 1/r$, (Fig. 2c) the particle cloud becomes highly sheared. On the second passage through the boundary current the cloud takes on a characteristic spiral shape with particles on inner streamlines circulating faster than those farther out (Fig. 2d).

The dispersion *across* and *along* streamlines can be measured by the second moments of displacement about the mean position of the group of particles; that is,

$$R_\psi = \frac{1}{N} \sum_{\text{all particles}} (\Psi_n - \bar{\Psi})^2$$

and

$$R_\theta = \frac{1}{N} \sum_{\text{all particles}} (\Theta_n - \bar{\Theta})^2,$$

where (Ψ_n, Θ_n) is the position in (ψ, θ) space of individual particles with the mean position of the cloud being $(\bar{\Psi}, \bar{\Theta})$; N is the number of particles. To obtain stable statistics it was found necessary for N to be around 5000. Because Θ_n is modulo(2π) the value of $\bar{\Theta}$ can be dependent on the position of the cloud on the gyre if Θ_n is measured relative to a fixed value of θ. To overcome this the mean is computed by measuring Θ_n relative to the position of the maximum in the distribution of particles.

The evolution with time of the rms spread of the particles $R_\psi^{1/2}$ and $R_\theta^{1/2}$ is shown in Fig. 3 for a number of values of A and n. The Péclet number is set at 500. The numerical experiments are divided into two groups: 1) fixed n with varying A corresponding to a fixed boundary length but varying width and 2) fixed A with varying n, fixed boundary width but varying length. The axisymmetric gyre (no boundary current) corresponds to $A = 0$ and $n \to \infty$ in the two groups, respectively. The characteristics of each gyre referred to the streamline $\psi = 1$ are given in Table 1, namely the circulation time T_c, the length of the boundary layer $\mathcal{L}$, and the fraction of circulation time spent within the boundary layer t_b. Here we have defined the boundary layer as being the region of a streamline for which the velocity is within 50% of the maximum velocity $U_{\max}$. For $\psi = 1$ then for Gyre 1, $U_{\max} = 1 + A$. The fractional time spent by particles within the boundary layer is relatively small. Even for the longest boundary layer considered ($n = 2$) a particle will spend only 6% of its time within the boundary layer.

The effect of the boundary layer is clearly seen in both R_ψ and R_θ (Fig. 3). Each passage through the boundary layer, as the streamlines are brought closer together, produces a sharp increase in R_ψ and a marked increase in the overall spreading rate across streamlines. There is a corresponding increase in R_θ as the particle cloud enters the boundary layer. This is, however, followed by a sharp decrease as the particle cloud exits the boundary layer. Interestingly, for the relatively short boundary layer with $n = 8$ the net effect on the along-streamline spread is minimal with the rate of increase in R_θ being little changed from that of the axisymmetric gyre ($A = 0$). Although the boundary layer produces large changes in R_θ, it is the shear in the recirculation region that plays the major part in the net along-streamline spreading.

To illustrate the point further a second gyre, Gyre 2, is considered such that

$$\psi = -\frac{e^{r^2 h(\theta)/2} - 1}{h(\theta)} \tag{8}$$

$$r = \left[\frac{2}{h(\theta)} \ln(1 - \psi h(\theta))\right]^{1/2} \tag{9}$$

with

$$u_\theta = -re^{r^2 h(\theta)/2}. \tag{10}$$

We will use the same shape function $h(\theta)$ as in Gyre 1, namely, expression (7). With $A = 0$, Gyre 2 is in solid body rotation, which implies no shear-induced dispersion. The along streamline spread, $R_\theta^{1/2}$, is shown in Fig. 4 for $A = 0$ and 6. With no shear in the recirculation region, the along-streamline spreading is much reduced from that of Gyre 1 (even when $A = 0$). It now takes several passages through the boundary layer before along-streamline mixing is complete.

Rhines and Young estimate the time to mix along streamlines, T_a, to be given by

$$T_a = \left[\kappa\left\{\left\langle \frac{d}{dr}\left(\frac{1}{r}\frac{d\psi}{dr}\right)\right\rangle\right\}^2 \Big/ 3\right]^{-1/3},$$

TABLE 1. Characteristics of the model Gyre 1 [defined by Eq. (4)]. Here A and n are gyre parameters, T_c is the circulation time, $\mathcal{L}$ is the length of the boundary layer, t_b is the fraction of circulation time spent within the boundary layer, T_a is the along-streamline mixing time given by RY, K_ψ the across-streamline diffusion coefficient and γ the parameter in (12).

A	n	T_c	$\mathcal{L}$	t_b	T_a (RY)	$K_\psi/U_0^2\kappa$	γ
0	—	6.3	0.0	0.0	14.4	1	—
2	8	5.8	0.53	0.044	13.8	1.7	2.1
4	8	4.6	0.40	0.024	13.0	2.0	1.9
6	8	3.5	0.37	0.017	11.8	2.6	2.1
6	4	4.6	0.46	0.032	12.8	3.9	2.4
6	2	1.7	0.60	0.063	10.6	7.2	2.2

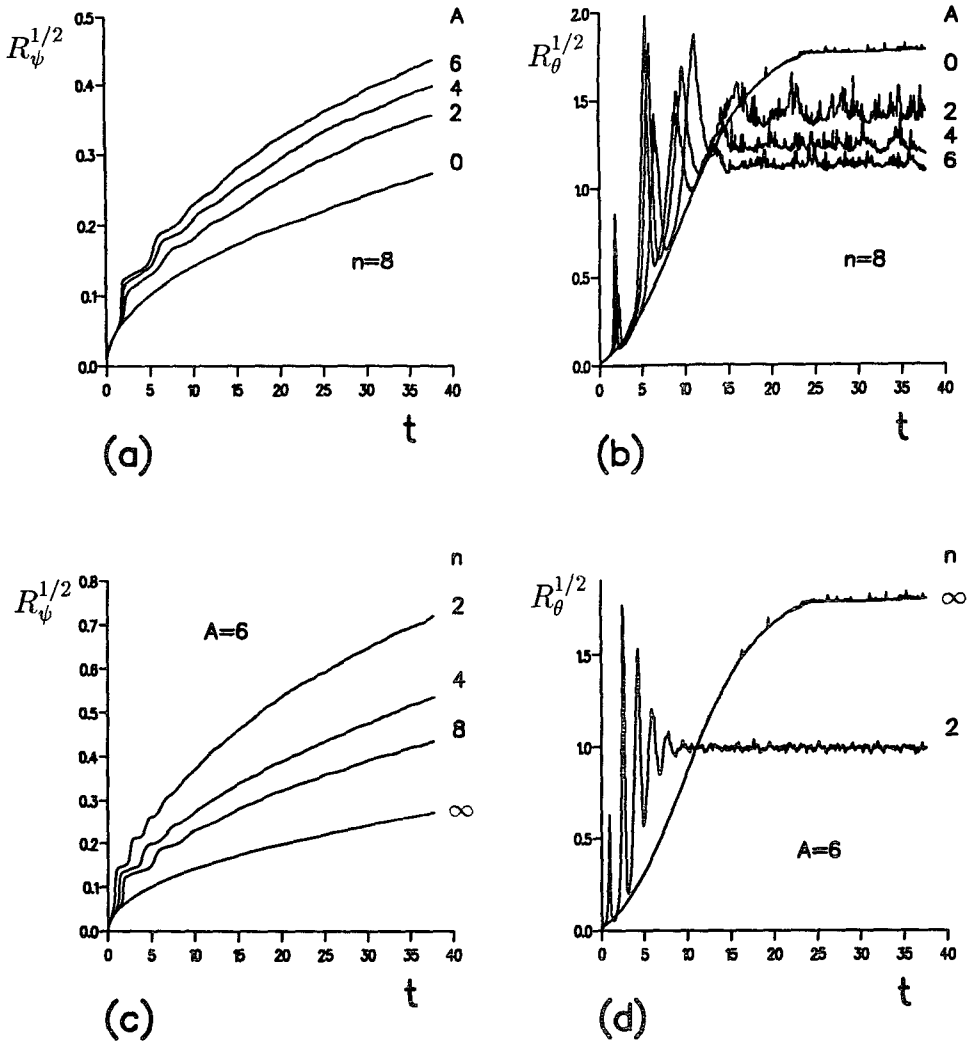

FIG. 3. Standard deviation of the particle cloud across, $R_\psi^{1/2}$, and along, $R_\theta^{1/2}$, streamlines in Gyre 1 as a function of time for varying boundary-layer strength A and length n; Pe = 500.

where angle brackets signify an along-streamline average. Their estimate for Gyre 1 is given in Table 1. When compared to Figs. 3b,d, the RY estimate is found to be reasonable, although the variation of mixing time with boundary-layer strength using RY is less than the numerical results. (Obtaining a precise value of mixing time from Figs. 3b,d is complicated by the large variations in R_θ during passage through the boundary layer.) The mixing time is somewhat overestimated for the longer and more intense boundary layers. This discrepancy should be expected as the value of $\langle d/dr(1/r d\psi/dr)\rangle$ is a function of r, and even with Pe = 500 there is considerable spreading across streamlines before the along-streamline mixing is complete.

The across streamline spread $R_\psi^{1/2}$ (Figs. 3a,c) is found to follow a $\sqrt{t}$ law to a good approximation. We can then define an effective across-streamline diffusion coefficient K_ψ such that

$$R_\psi^{1/2} = \sqrt{K_\psi t}.$$

The value of K_ψ relative to the background diffusion coefficient κ is given in Table 1. With $A = 6$, $n = 2$ the effect of the boundary layer is to increase the effective diffusion coefficient sevenfold.

After the tracer has been mixed along streamlines, Y shows that the evolution of a tracer field, $C(t)$, will follow

$$\frac{\partial C}{\partial t} = \frac{\partial}{\partial \mathcal{A}}\left[K_{\mathcal{A}} \frac{\partial C}{\partial \mathcal{A}}\right],$$

where $\mathcal{A}$ is the area enclosed by a streamline and the diffusion coefficient $K_{\mathcal{A}}$ is given by

$$K_{\mathcal{A}} = \kappa \oint |\text{grad}\psi|\, dl \oint \frac{dl}{|\text{grad}\psi|}. \qquad (11)$$

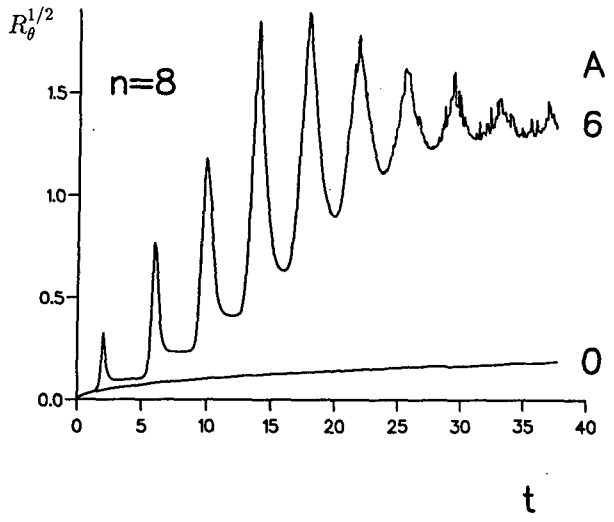

FIG. 4. Along-streamline standard deviation of the particle cloud, $R_\theta^{1/2}$, in Gyre 2 as a function of time for $A = 0, 6$; $n = 8$, Pe = 500.

If $\psi \sim r$, then the two diffusion coefficients K_ψ and $K_{\mathcal{A}}$ are related by

$$K_\psi \approx \frac{\psi^2}{4\mathcal{A}^2} K_{\mathcal{A}}.$$

Note that with $\psi \sim r$, then $K_{\mathcal{A}} \sim r^2$, whereas K_ψ remains approximately constant with r making K_ψ a better measure of cross-streamline diffusion.

Since the spacing between streamlines is inversely proportional to the speed of the flow we can use the following as a crude model for the effective cross-streamline diffusion coefficient:

$$K_\psi \approx U_0^2 \kappa \left[(1 - t_b) + \gamma \left(\frac{U_{\max}}{U_0} \right)^2 t_b \right], \quad (12)$$

where U_0 is a reference velocity in the recirculation region, t_b the fraction of the circulation time spent within the boundary layer, and γ a parameter.

Here we have split the flow into two regions: 1) the boundary layer where the spacing between streamlines $\sim 1/U_{\max}$ and 2) the recirculation region where the spacing $\sim 1/U_0$. The parameter γ is determined by fitting (12) with the numerical results.

Expression (11) is related to (12), since

$$\oint \frac{dl}{\text{grad}\psi} \sim \frac{L}{U_0} \quad \text{and} \quad \oint \text{grad}\psi dl \sim \mathcal{L} U_{\max},$$

and

$$\frac{U_{\max}}{U_0} \sim \frac{L}{l} \quad \text{and} \quad t_b \sim \frac{\mathcal{L} U_0}{U_{\max} L},$$

where the horizontal scale of the gyre is denoted by L and the boundary-layer width by l.

Fitting (12) to the Gyre 1 results we find that γ is approximately a constant of value 2 (see Table 1), indicating that indeed expression (12) is a useful model for the effective diffusion coefficient of the gyre. Noting that the second term in the square brackets on the rhs of (12) dominates for gyres with narrow boundary layers, we can express (12) in terms of the time for the tracer to become well mixed across the gyre, T_{mix}. Thus, as $T_{\text{mix}} \sim \psi_0^2 / K_\psi$, where ψ_0 ($\sim U_0 L$) is the streamfunction on the boundary, we expect

$$T_{\text{mix}} \sim \frac{lL^2}{\mathcal{L}\kappa},$$

or

$$T_{\text{mix}} \sim \frac{lL}{\mathcal{L} U_0} \text{Pe}. \quad (13)$$

The mixing time is therefore dependent on three length scales; the gyre scale L, the boundary-layer width l, and the boundary length $\mathcal{L}$. This is a simple extension of Y's result, who implicitly assumes $\mathcal{L} \approx L$. We will test the validity of (13) in section 3.

b. *More general gyres*

The above model gyres have been useful in elucidating the effects of gyre shape on the dispersion of a tracer. Often, however, we are interested in the dispersion characteristics of a particular gyre that may be the consequence of a given forcing field, such as the wind-driven Stommel gyre considered below. In addition, in order to study the final stages of mixing and, in particular, low Péclet number flows the gyre needs to be placed in a closed domain with boundaries. We will assume we have a specified streamfunction field, here given in Cartesian coordinates,

$$\psi = G(x, y). \quad (14)$$

We will generalize the position on a given streamline θ by relating it to the distance d along the streamline from some fixed point. We therefore define θ by

$$\theta = \frac{2\pi d}{D},$$

where D is the total length of the streamline. Then $0 \leq \theta \leq 2\pi$. As before we require mappings between the two spaces (x, y) and (ψ, θ). In general, these have to be constructed numerically on grids in both spaces. We also require the rate of change of position along a streamline $\partial\theta/\partial t$. Details of the numerical procedure are given in appendix A.

Figure 5 shows the lines of constant streamfunction and θ in (x, y) space for the Stommel gyre:

$$\psi = A(1 + C_1 e^{\lambda_1 x} + C_2 e^{\lambda_2 x}) \sin(\pi y) \quad (15)$$

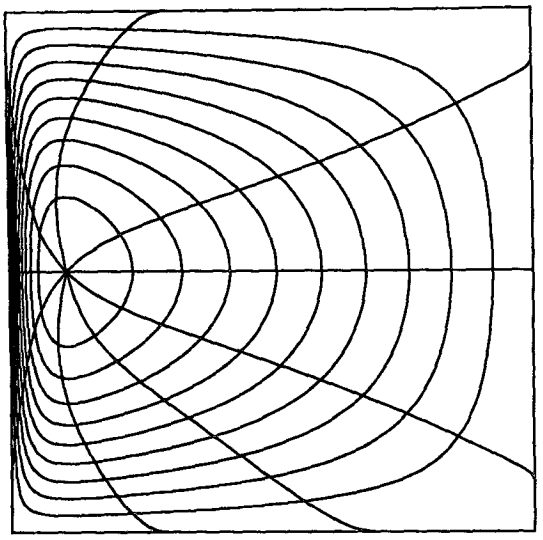

FIG. 5. Numerically generated streamline coordinate grid ψ, θ for a Stommel gyre with $\epsilon = 0.03$.

defined on

$$0 \leq x \leq 1, \quad 0 \leq y \leq 1,$$

where

$$\lambda_1 = \frac{-1 + (1 + 4\pi^2\epsilon^2)^{1/2}}{2\epsilon},$$

$$\lambda_2 = \frac{-1 - (1 + 4\pi^2\epsilon^2)^{1/2}}{2\epsilon},$$

and

$$C_1 = \frac{1 - e^{\lambda_2}}{e^{\lambda_2} - e^{\lambda_1}}, \quad C_2 = \frac{-1 + e^{\lambda_1}}{e^{\lambda_2} - e^{\lambda_1}}.$$

(Stommel 1948). This corresponds to an ocean in a square basin driven by a sinusoidal wind stress with bottom friction acting as the dissipative mechanism. The maximum absolute value of the streamfunction is set to one. The horizontal length scale L is taken to be the width of the square box. The parameter ϵ represents the width of the boundary layer. In Fig. 5 it is set to 0.03. With a narrow boundary current, the nondimensional velocity in the recirculation region U_0, the Sverdrup velocity, is then approximately $U_0 \approx \psi_{\max} = 1$. With $\epsilon = 0.03$, the maximum velocity in the boundary layer is 37.3, which occurs on $\psi = 0$ on the western boundary.

As before we will present the results of the random walk model in terms of R_ψ and R_θ. Figure 6 shows the same for two different Péclet numbers, Pe = 40 and 400. These Péclet numbers, for this gyre, correspond to the strong and weak diffusion regimes of Y, respectively. We will be rather more precise about differentiating between the two regimes in the next section. The release point for the particles was $(x, y) = (0.125, 0.25)$ ($\psi = 0.70$). This is in the entrance region to the boundary current (Fig. 5). To compare with the model Gyre 1, the maximum velocity on $\psi = 0.70$ is 12.6 and the fraction of time spent in the boundary layer, t_b, is 0.07.

With Pe = 400 the initial stage of mixing is similar to that of the model gyre with a similar Péclet number; that is, the particles are mixed along the streamline after a small number of passes through the boundary current. Subsequent mixing occurs across streamlines with R_ψ varying linearly with time. The effective diffusion coefficient $K_\psi / U_0^2 \kappa$ is 9.2. Fitting expression (12) to this value we find $\gamma \approx 0.68$. Varying the width of the boundary layer for the Stommel gyre does not significantly change the value of γ. With $\epsilon = 0.1$ and 0.01, then in the weak diffusive regime γ was found to be 0.89 and 0.71, respectively. When comparing the Stommel gyre results with those of the model gyre pre-

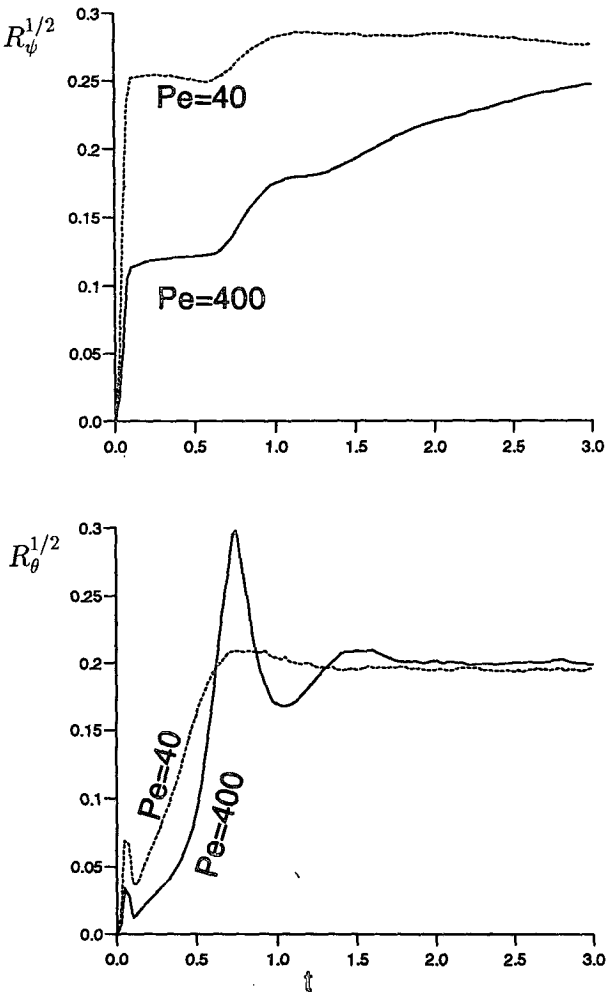

FIG. 6. Variance of particle positions (a) across R_ψ and (b) along R_θ streamlines in a Stommel gyre against time with Pe = 40 and Pe = 400.

sented in Table 1 we need to take note that the effective Péclet number, K_ψ/U_0^3L, is scaled with the width of the box for the Stommel gyre and the maximum distance from the streamline on which the tracer is released to the center of the gyre for the model gyre (in this case a third of the total width of the box). Thus, γ in Table 1 should be divided by a factor of approximately 3. The two gyres then give very similar results. The very close agreement is perhaps somewhat fortuitous but it does show the relevance of the model gyre results.

At later times the rate of increase of R_ψ decreases and the value of R_ψ tends to a constant as the particles become uniformly spread across the basin.

The lower Péclet number case (Pe = 40) behaves somewhat differently. Now it takes only one to two passes through the boundary layer before mixing is accomplished along streamlines. After one pass through the boundary layer there has been a significant spread across streamlines and R_ψ is within 10% of its final value. There is now no intermediate state in which R_ψ goes as t. The time to reach a mixed state has been much reduced.

In order to delineate the various mixing regimes we need to define a mixing time. We choose to do this in terms of the uniformness of the tracer concentration. To convert particle density to tracer concentration requires a much larger number of particles than we have been using. This is because the particle density reduces as the particles are spread over the gyre and it is sometime before some regions of the outer recirculation receive a sufficient number to obtain stable statistics. To continue, in the next section we consider a continuous model.

Another reason for changing to a continuous model is that the routine for generating the numerical (ψ, θ) grid was found to breakdown for very nonlinear gyres, such as that considered in section 3. The reason for this breakdown is that the grid in x, y space becomes very distorted and numerical inaccuracies dominate. The solution is either a change in the numerical technique for the grid generation or a change in the definition of θ. To date no satisfactory way forward has been found.

3. Continuous model

The horizontal distribution of a continuous tracer $C(x, y)$, advected by a steady velocity field with streamfunction $\psi(x, y)$ and diffused by a constant eddy diffusivity κ satisfies the advection–diffusion equation

$$\frac{\partial C}{\partial t} + \frac{\partial \psi}{\partial y}\frac{\partial C}{\partial x} - \frac{\partial \psi}{\partial x}\frac{\partial C}{\partial y} = \frac{1}{\mathrm{Pe}}\nabla^2 C, \qquad (16)$$

where, as before, we normalize the streamfunction such as to have a maximum absolute value of 1 and nondimensionalize length with the basin width L. Then the Péclet number is given by $\mathrm{Pe} = U_0 L/\kappa$, where $U_0 = |\psi^*_{\max}|/L$ (the asterisk denoting dimensional streamfunction).

We will impose a zero normal gradient, $\partial C/\partial n$, on the boundaries $x = 0, L$ and $y = 0, L$ which is equivalent to imposing a no-flux condition.

Equation (16) is solved numerically with a given streamfunction field. The horizontal variation of the tracer, C, and the streamfunction ψ are treated spectrally in terms of Chebyshev polynomials (see appendix B). The Chebyshev spectral method was found to perform well in resolving the tracer field in flows with narrow boundary layers. Typically the number of Chebyshev modes (in any spatial dimension) required by the spectral model to adequately resolve the tracer field was less than half the number required by a finite difference model (e.g., see Musgrave 1985).

Numerical experiments were performed with a Stommel gyre [Eq. (15)] with varying width; $\epsilon = 0.1$, 0.03, and 0.01. The initial tracer field in all experiments was taken to be a Gaussian "blob" with an e-folding radius of 0.035 centered at $(x, y) = (0.125, 0.25)$; the same location as in the random walk experiments. The finite width of the initial tracer field has consequences for the dispersion during the first pass through the boundary layer. The dispersion rates being higher than for a point release. Apart from this the results are essentially the same as the random walk model.

We present the results from two experiments in terms of the second-order moments in (x, y) space; namely,

$$R_{xx} = \frac{\langle (x - x_c)^2 C\rangle}{\langle C\rangle}, \quad R_{yy} = \frac{\langle (y - y_c)^2 C\rangle}{\langle C\rangle},$$

where (x_c, y_c) is the location of the center of mass of the tracer.

The results for the Stommel gyre with the boundary-layer width set at the same value as the random walk model in section 2b $\epsilon = 0.03$ and Pe = 40 and 400 are shown in Fig. 7. The form of the curves of the statistics in (x, y) space should be compared to that in (ϕ, θ) space, (Fig. 6). (A direct comparison between the continuous and random walk models, taking into account the different initial distributions, gives a good agreement between the two model results). As before, the low Péclet number regime rapidly mixes the tracer across the basin. The equilibrium value of R_{xx} and R_{yy} corresponding to a uniform tracer distribution is $1/12$. The rapid rise of R_{yy} corresponds to the tracer being pulled out by the high shear on its first passage through the boundary current. The subsequent rise in R_{xx} is associated with the alignment of the tracer field as it circulates around the gyre. In contrast, the high Péclet number case shows much less spreading on the first pass through the boundary layer due to the reduced dispersion across streamlines before entering the boundary layer. On its second passage the tracer is

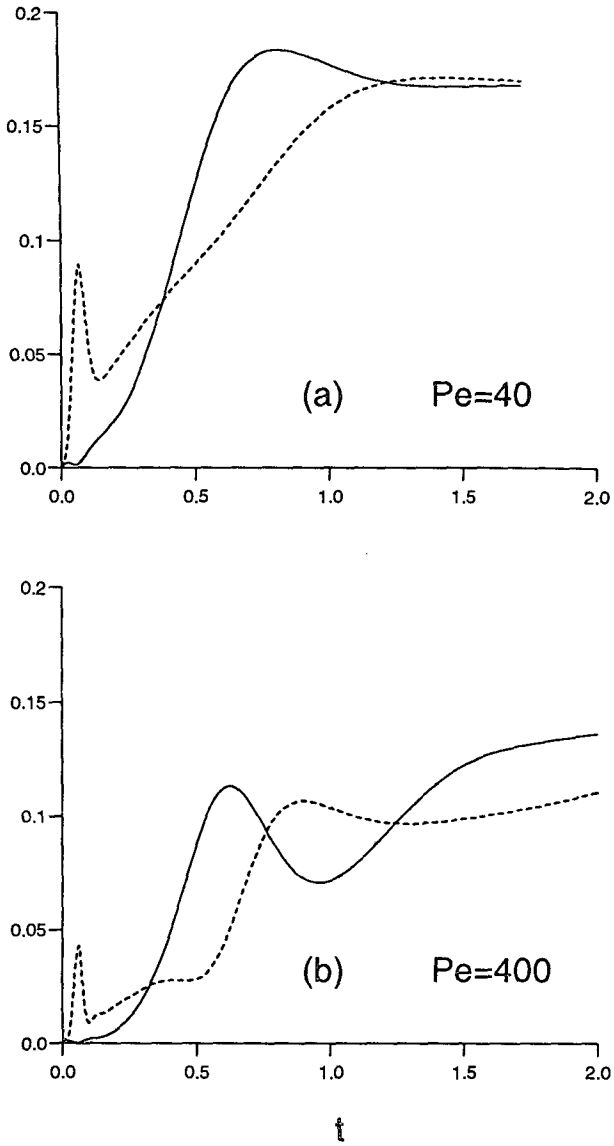

FIG. 7. Evolution of the second-order moments R_{xx} (solid line) and R_{yy} (dashed line) for a Stommel gyre with $\epsilon = 0.03$: (a) Pe = 40, (b) Pe = 400.

pulled out first in x and then y. The effective diffusivity during these periods of rapid increase in R_{xx} and R_{yy} is some 10 times the explicit diffusivity. However, neither R_{xx} nor R_{yy} are monotonic. Both show periods of rapid decrease or an effective "negative" diffusion. Estimating an overall effective diffusivity is somewhat meaningless and misleading, highlighting the desirability of working in (ψ, θ) space. After approximately $t = 1.5$ (see Fig. 6) the tracer has become well mixed along streamlines and evolves slowly to a well-mixed state.

Although statistics in (x, y) space have some undesirable characteristics during the early evolution of the tracer field, they are useful in indicating how uniformly spread the tracer is across the basin [unlike statistics in (ψ, θ), which are dependent on the gyre shape]. One way to characterise the effectiveness of a gyre to mix a tracer is to define a mixing time. We will define the mixing time of the gyre, T_{mix}, as the time at which the variation of the tracer distribution across the basin is less than 10%. The mixing time as a function of Péclet number is shown in Fig. 8 for the three Stommel gyres. The two gyres with the narrower boundary current ($\epsilon = 0.03$ and 0.01) exhibit three distinct mixing regimes. At very low Péclet number the system is dominated by diffusion alone. At high Péclet number the mixing time increases linearly with Pe. This corresponds to the "weak" diffusive regime of Y (rapid mixing along streamlines, slow mixing across). At intermediate values of Pe, T_{mix} is independent of Pe, the "strong" diffusive limit (rapid mixing across streamlines). For the wide boundary-layer case ($\epsilon = 0.1$) the intermediate regime is not distinct.

The value of the streamfunction passing through the release point of the tracer is $\psi = (0.60, 0.70, 0.66)$ for the three gyres with ϵ or $l/L = (0.1, 0.03, 0.01)$. The corresponding length of the boundary layer $\mathcal{L} = (0.53, 0.46, 0.46)$, where $\mathcal{L}$ is defined, as before, as the length of the streamline for which the velocity is within 50% of its maximum value. Using (13) we therefore expect the slope of the linear part of the T_{mix} versus Pe curve (the weak regime) for the three gyres to be in the ratio (2.9:1.0:0.33). [Here we have normalized the slope with the value for $\epsilon = 0.03$ since (13) gives us how the slope is expected to vary with gyre geometry not the absolute slope.] The slopes from the numerical experiments are in the ratio (1.2:1.0:0.35). The variation in mixing time with l/L is therefore in accord with (13)

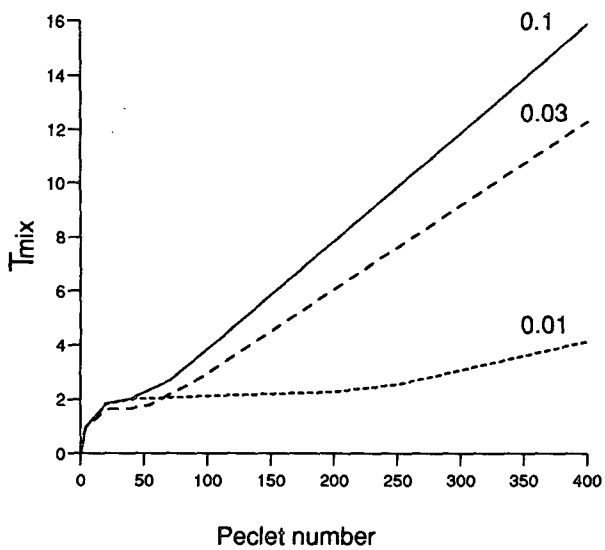

FIG. 8. Mixing time plotted as a function of Pe for the Stommel gyre for varying boundary-layer widths.

for the two narrower boundary-layer cases. The mixing time for the wide boundary-layer case is smaller than the value given by (13); not unexpected as (13) assumes cross-streamline mixing occurs only in the boundary layer.

The transition between the strong and weak diffusive regimes occurs at a similar value of (l/L) Pe for the gyres with $\epsilon = 0.03$ and 0.01, the transition occuring at approximately 1.8 and 2.4, respectively. Y puts the condition for the strong regime as $\mathrm{Pe} \gg 1 \gg (l/L)$ Pe. The numerical experiments show that the strong regime extends to somewhat greater values of the Péclet number than suggested by the strict limits of the analysis of Y.

The final gyre we will consider we will call the nonlinear gyre and is shown in Fig. 9. It is in fact the mean surface streamfunction from an eddy-resolving quasi-geostrophic model developed by Rogers and Richards (1988). (The *qg* model again uses Chebyshev polynomials in the horizontal with normal modes in the vertical.) The gyre has an extended boundary layer, a tight inertial recirculation region, and a slower, more linear, recirculation over the rest of the basin. The characteristics of the gyre are typical of this type of ocean model. To compare with the Stommel gyre, the boundary layer width l/L is approximately 0.03 and, for $\psi = 0.35$, the streamline passing through the release point $(x, y) = (0.125, 0.25)$, the boundary length $\mathcal{L}$ is 1.23. The gyre therefore has a boundary layer of width comparable to the second of the Stommel gyres but is some 2.5 times longer in length.

The evolution of the tracer field is shown in Fig. 10 for the release of the tracer cloud at two positions. The Péclet number is 400. The figure shows the tracer fields after approximately one, two, and four passages through the boundary layer. The first release point is the same as that used for the Stommel gyres, namely, $(x, y) = (0.125, 0.25)$, which places the tracer on a streamline ($\psi = 0.35$) that passes through the linear part of the gyre. The second is at $(x, y) = (0.125, 0.75)$, which is in the inertial part of the gyre (on $\psi = 0.72$). The mixing times for the two releases are 2.93 and 8.32, respectively. The mixing time for the Stommel gyre with $l/L = 0.03$ at the same Péclet number is 12.27. The reduction in mixing time for the nonlinear gyre is consistent with the increase in boundary-layer length (Eq. 13). The boundary-layer lengths $\mathcal{L}$ are 0.46 for the Stommel gyre and 0.8 and 1.25 for the nonlinear gyre for the streamlines passing through the inner, $(x, y) = (0.125, 0.75)$, and outer, $(x, y) = (0.125, 0.25)$, release points, respectively. The product $T_{\mathrm{mix}}\mathcal{L}$ is then 5.6, 6.6, and 3.6 for the three cases, respectively. The first two values are approximately constant, which is consistent with the scaling suggested by (13). Case 3, the release on the outer streamline of the nonlinear gyre, gives a reduced value for the product $T_{\mathrm{mix}}\mathcal{L}$. Because of the increase length of the boundary layer for this release point the system is not in the weak regime

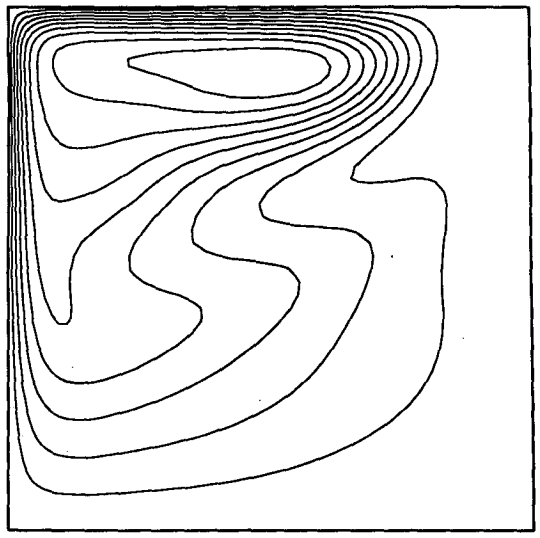

FIG. 9. Streamfunction field for the nonlinear gyre used in the numerical experiments.

with Pe = 400 (additional experiments showed that for this release point T_{mix} is approximately constant with Pe for values of Pe up to at least 400).

The evolution of the tracer fields for the two releases in the nonlinear gyre is very different. The tracer placed in the inertial part of the gyre, as with the linear gyres, mixes quickly along streamlines such that after four passes through the boundary layer the tracer distribution reflects the streamfunction (see Fig. 11). The tracer placed in the linear part of the gyre looks very different. Now the maximum in the tracer concentration is toward the southern boundary of the gyre and there are a series of ridges and valleys in the tracer field. The tracer field toward the center of the gyre is uniform. The ridges are formed by successive passes of the tracer cloud through the boundary layer. As before with the linear gyre the reduction in circulation time toward the center of the gyre causes the tracer distribution to take on a spiral shape. Here, because the streamlines separate sharply after exiting the boundary layer and the flow on the outer streamlines is relatively slow the arms of the spiral are quite distinct. The presence of the boundary is also having an effect on the distribution. This once again highlights the importance of the shape of the recirculation region of the gyre in the evolution of a tracer field. (A similar effect, but not so marked, is also found with the Stommel gyre if the tracer is released very close to the boundary.)

4. Conclusions

We have presented a number of simple models to study the dispersion of a tracer by a two-dimensional gyre circulation. We have found that the dispersion by a given gyre can be characterized in terms of a bulk Péclet number and the three length scales, L the hor-

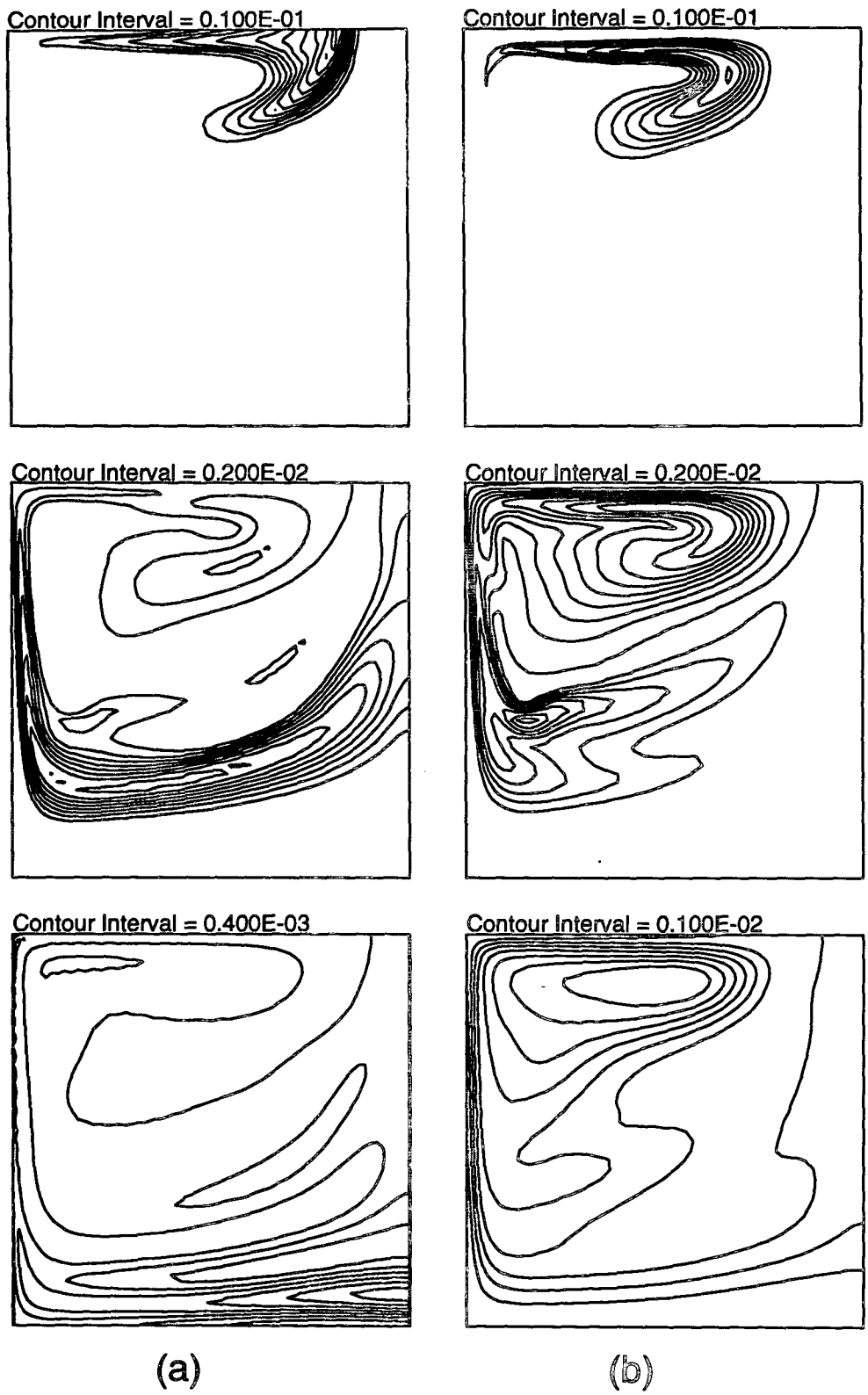

FIG. 10. Evolution of the tracer field in the nonlinear gyre for different initial positions: (a) outside and (b) inside the inertial recirculation region for times t = 0.2, 1.0, and 2.4.

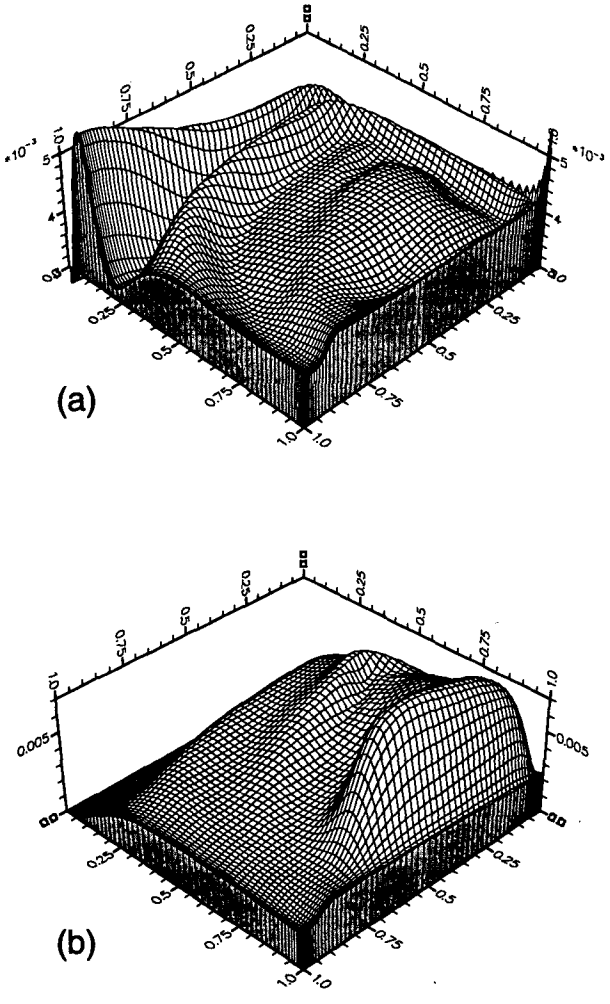

FIG. 11. Perspective plot of the tracer concentration at $t = 2.4$ for the two cases shown in Fig. 10 viewed from the northwest corner of the basin.

izontal width of the gyre, l the width of the boundary current, and $\mathcal{L}$ the length of the boundary current. By taking into account the length of the boundary layer, gyre dispersion is found to conform moderately well with the analytic models of RY and Y, in particular the partitioning between weak and strong diffusive regimes suggested by Y, even though the shear characteristics may be quite variable across the gyre. The analytic models become less valid as the length of the boundary layer increases.

The expressions (12) and (13) for the cross-streamline diffusion coefficient and mixing time, respectively, have been found to be useful estimates in gyres of varying shape at high Péclet number (the weak regime of Y).

Young's strong regime is found to extend to higher Péclet numbers than suggested by the limits of the analytic model. Recent estimates of ocean Péclet numbers put Pe at around 10 for the midthermocline (see, e.g., Musgrave 1990). For the North Atlantic subtropical gyre $l/L \approx 0.03$. The value for l Pe$/L$ is then 0.3 putting the gyre in the strong, rapid mixing regime. Ocean gyres appear to be efficient mixers. The reader is cautioned, however, as the estimates of Péclet in the ocean are very crude and so much depends on gyre geometry and source location.

A major conclusion to come out of this study is the importance of the shape of the recirculation region. The initial mixing along streamlines is very dependent on the shear in this region. Indeed in most cases the boundary layer was found to have a minor role in the spreading of tracer along streamlines. Even at large times the shear in the recirculation can be important (see Fig. 11). This puts into question conclusions drawn from using simple Stommel gyres in comparisons with observed tracer distributions. A given ocean gyre will have an effective Péclet number that varies not only from streamline to streamline but also along individual streamlines (provided of course that the concept of eddy diffusion is valid). The distribution of a tracer will depend on where it is input in relation to the distribution of shear. If the tracer is injected through the upper mixed layer the tracer distribution on a given density surface will therefore be very dependent on the shape of the outcrop line of that surface and the isopycnic shear of the circulation. The effect of the form of injection of the tracer and an extension to a 3D circulation model of the flow in the North Atlantic with transient tracers will be examined in a future paper.

Acknowledgments. This work was part funded by the NERC under Grant GR3/6219. Assistance by Dr. S. O'Farrell in running early versions of the continuous model is greatfully acknowledged.

APPENDIX A

Transformation between (x, y) and (ψ, θ) Coordinates: Numerical Grid Generation

Here we describe the method used in generating a (ψ, θ) grid for a general gyre shape and the transformations between (x, y) and (ψ, θ) spaces. It is assumed that the gyre circulation is closed and is in an enclosed domain.

The streamfunction $\psi(x, y)$ for the flow field is assumed to be a known analytic function or defined on a given (x, y) grid. The maximum value of the streamfunction at the center of the gyre will be set to one, and to zero along the boundaries.

The coordinate θ represents the position on a given streamline and is defined as

$$\theta = \frac{2\pi d}{D},$$

where D is the total length of the streamline and d is the distance along the streamline from a fixed starting point. Thus, d ranges from zero to 2π. In general, for a given streamline the function $d(x, y)$ will not be known analytically.

a. Generation of a (ψ, θ) grid from $\psi(x, y)$

We define the streamfunction $\psi(x_i, y_j)$ on a grid (x_i, y_j) $(i = 1, I; j = 1, J)$ in (x, y) space. The contour ψ_n $(n = 1, N)$ is then defined as the piecewise linear curve determined by the intersection of the isoline of ψ with the (x_i, y_j) grid. Dividing the contour ψ_n into M equal length segments, we can construct the grid (ψ_n, θ_m), $(n = 1, N; m = 1, M)$, with known corresponding points in (x, y) space, $(x(\psi_n, \theta_m), y(\psi_n, \theta_m))$. For a sufficiently fine grid in (x, y) space linear interpolation is found to suffice. An example of a coarse (ψ_n, θ_m) grid in (x, y) space for a Stommel gyre is given in Fig. 5.

b. Transforming from (ψ, θ) space to (x, y) space

The simplest way of finding (x, y) from any given (ψ, θ) is by bilinear interpolation from the distribution $(x(\psi_n, \theta_m), y(\psi_n, \theta_m))$. Thus, for a value of (ψ, θ) located within a grid box bounded by ψ_{n1}, ψ_{n2} and θ_{m1}, θ_{m2}, such that

$$\psi_{n1} \geq \psi > \psi_{n2}, \quad \theta_{m1} \leq \theta < \theta_{m2},$$

(see Fig. A1) then (x, y) is given by

$$x = (1 - p)(1 - q)x_2 + (1 - p)qx_4 + p(1 - q)x_1 + pqx_3 \quad \text{(A1)}$$

$$y = (1 - p)(1 - q)y_2 + (1 - p)qy_4 + p(1 - q)y_1 + pqy_3, \quad \text{(A2)}$$

where

$$p = \frac{(\psi - \psi_{n2})}{(\psi_{n1} - \psi_{n2})}, \quad q = \frac{(\theta - \theta_{m1})}{(\theta_{m2} - \theta_{m1})}.$$

c. Transforming from (x, y) space to (ψ, θ) space

Care needs to be exercised when transforming back to (ψ, θ) space. Because the streamlines are curved the point $P_2 = (x, y)$ calculated from (A1), (A2) will, in general, be different from the true position P_1 (see Fig. A1). Repeated transforms between the two spaces can therefore cause an unacceptable displacement of a particle (for example, for the Stommel gyre, 1000 transforms produced a displacement across 10% of the basin width).

The solution is to perform all interpolations in the same space. Thus, for a given point (x, y), the (ψ, θ) grid box in which the point is located is determined: the grid box in (x, y) space is defined as the quadrilateral ABCD (Fig. A1). The value of (ψ, θ) is then determined by inverting (A1), (A2). In general, this inversion requires an iterative method and can be very time consuming.

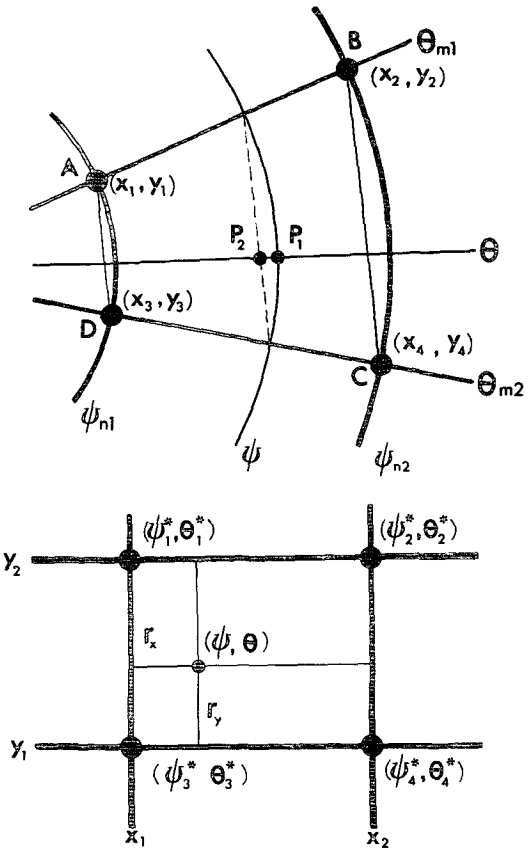

FIG. A1. Schematic presentation of bilinear interpolation transformations between (ψ, θ) and (x, y) spaces.

The compromise adopted here was to generate a new set of values $\psi^*(x_i, y_j)$ and $\theta^*(x_i, y_j)$ at the grid points of the (x, y) grid. Equations (A1) and (A2) were inverted using a Newton–Raphson method at each of the grid points (x_i, y_j). Transforms back to (ψ, θ) were then performed on the (x, y) grid using the new values (ψ^*, θ^*). Thus, for any given (x, y), where

$$x_i \leq x < x_{i+1}, \quad y_j \leq y < y_{j+1},$$

then

$$\psi = (1 - r_x)(1 - r_y)\psi_3^* + (1 - r_x)r_y\psi_1^* + r_x(1 - r_y)\psi_4^* + r_x r_y \psi_2^* \quad \text{(A3)}$$

$$\theta = (1 - r_x)(1 - r_y)\theta_3^* + (1 - r_x)r_y\theta_1^* + r_x(1 - r_y)\theta_4^* + r_x r_y \theta_2^*, \quad \text{(A4)}$$

where

$$r_x = \frac{(x - x_i)}{(x_{i+1} - x_i)}, \quad r_y = \frac{(y - y_j)}{(y_{j+1} - y_j)}.$$

This method was found to drastically reduce the error in repeated transforms. For the Stommel gyre with (x, y), (ψ, θ) grids with $I, J, N, M \approx 100$, the displacement after 1000 repeated transforms was less than one grid interval (less than a random jump). The standard deviation between ψ and ψ^* at the (x_i, y_j) points was 3×10^{-4}.

APPENDIX B

Spectral Model for a Continuous Tracer Field

In solving (16) numerically we represent the horizontal variation of both the tracer field C and the streamfunction ψ by spectral methods. In an enclosed ocean domain the Chebyshev polynomials, $T_n(\cos\theta) = \cos n\theta$, are an attractive set of orthonormal spectral functions (Gottlieb and Orszag 1977). Furthermore, for the application of mixing in narrow boundary currents the nonuniform resolution associated with the Chebyshev polynomials can be expected to offer significant advantages. Consequently, we represent the tracer field as the spectral expansion

$$C(x, y, t) = \sum_{n=0}^{N_x} \sum_{m=0}^{N_y} C_{n,m}(t) T_n(x) T_m(y),$$

where $N_x + 1$ modes describe the variation in the E–W direction, etc. Transforms between coordinate space arrays and spectral coefficients are performed by means of double cosine transforms based on FFT algorithms. Functions defined on the two-dimensional spatial grid

$$x_i = \frac{1}{2}\left[1 - \cos\left(\frac{\pi i}{N_x}\right)\right], \quad i = 0, \cdots, N_x$$

$$y_j = \frac{1}{2}\left[1 - \cos\left(\frac{\pi j}{N_y}\right)\right], \quad i = 0, \cdots, N_y$$

are transformed to spectral space using the relationship

$$C(x_i, y_j) = \sum_{n=0}^{N_x} \sum_{m=0}^{N_y} C_{n,m} \cos\left(\frac{\pi n i}{N_x}\right) \cos\left(\frac{\pi m j}{N_y}\right).$$

To implement the boundary conditions correctly in a spectral model (tau method) the diffusion term must be treated semi-implicitly. Representing the rate of change of tracer concentration by a "leap frog" approximation, the time step variables a and b may be introduced:

$$a = \nabla^2 C - \frac{\mathrm{Pe}}{\Delta t} C$$

$$b = \nabla^2 C + \frac{\mathrm{Pe}}{\Delta t} C,$$

giving the time step scheme

$$a^{n+1} = -b^{n-1} + 2\,\mathrm{Pe} J^n,$$

where J^n is the Jacobian $J(\psi, C)$ evaluated at the nth time step.

To determine the tracer concentration at the new time level the Helmholtz equation

$$\nabla^2 \eta^{n+1} - \frac{\mathrm{Pe}}{\Delta t} \eta^{n+1} = a^{n+1}$$

is solved by the method described by Haidvogel and Zang (1979). The tau method imposes the gradient boundary conditions as the constraints

$$\sum_{\substack{p=0 \\ \text{even}}} p^2 C_{p,m} = \sum_{\substack{p=1 \\ \text{odd}}} p^2 C_{p,m} = 0, \quad 0 < m < N_y$$

$$\sum_{\substack{p=0 \\ \text{even}}} p^2 C_{n,p} = \sum_{\substack{p=1 \\ \text{odd}}} p^2 C_{n,p} = 0, \quad 0 < n < N_x.$$

The advection of the tracer concentration is treated pseudospectrally. The spectral coefficients $J_{n,m}$ are determined from the flux form of the Jacobian; namely,

$$J_{n,m} = \{\partial_y(C\partial_x\psi) - \partial_x(C\partial_y\psi)\}_{n,m}.$$

The braces indicate that the Chebyshev transform is to be taken of the expression enclosed. The tracer fluxes are evaluated using the recursive algorithm for the derivative in the x direction:

$$C^{(x)}_{n,m} = C^{(x)}_{n+2,m} + (2n+1)C_{n+1,m}, \quad 0 \leq n \leq N_x + 1$$

with $C^{(x)}_{N_x,m} = C^{(x)}_{N_x+1,m} = 0$.

The flux form of the Jacobian ensures that the tracer concentration is conserved exactly since the discrete algorithm preserves $\langle J \rangle = 0$. Unfortunately, the algorithm does not guarantee $\langle CJ \rangle = 0$ exactly, owing to the Chebyshev nonuniform weight. Explicit evaluation of $\langle CJ \rangle$ indicates that it is generally two or more orders of magnitude smaller than the explicit diffusion coefficient $-\kappa\langle(\nabla C)^2\rangle$. However, since the term is not constrained to be exactly zero, experience has shown that some level of explicit diffusion is necessary to prevent the scheme from generating small-scale noise. Both terms are monitored throughout the integrations and for the range of explicit diffusion values examined here this has not proved a serious restriction. On this basis the effects of numerical diffusion are considered to be small in comparison with the levels of explicit diffusion studied.

REFERENCES

Allen, C. M., 1982: Numerical simulation of contaminant dispersion in estuary flows. *Proc. Roy. Soc. London,* **A381,** 179–194.

Gottlieb, D., and S. A. Orszag, 1977: *Numerical Analysis of Spectral Methods: Theory and Applications.* Soc. Ind. Appl. Math., Philadelphia, 170 pp.

Haidvogel, D. L., and T. Zang, 1979: The accurate solution of Poisson's equation by expansion in Chebyshev polynomials. *J. Comput. Phys.,* **30,** 167–180.

Jenkins, W. J., 1988: The use of anthropogenic tritium and helium-3 to study subtropical gyre ventilation and circulation. *Proc. Roy. Soc. London,* **A325,** 43–59.

Musgrave, D. L., 1985: A numerical study of the roles of subgyre-scale mixing and the western boundary current on homogenization of a passive tracer. *J. Geophys. Res.*, **90,** 7037–7043.

——, 1990: Numerical studies of tritium and helium-3 in the thermocline. *J. Phys. Oceanogr.*, **20,** 344–373.

Rhines, P. B., and W. R. Young, 1983: How rapidly is a passive scalar mixed within closed streamlines? *J. Fluid. Mech.*, **133,** 133–145.

Rogers, C. F., and K. J. Richards, 1988: On the vertical structure description of quasi-geostrophic ocean models. *Dyn. Atmos. Oceans,* **12,** 207–232.

Sarmiento, J. L., G. Thiele, R. M. Key, and W. S. Moore, 1990: Oxygen and nitrate new production and remineralization in the North Atlantic subtropical gyre. *J. Geophys. Res.*, **95,** 18 303–18 315.

Stommel, H., 1948: The westward intensification of wind-driven ocean currents. *Eos Trans. Amer. Geophys. Union,* **29,** 202–206.

Thiele, G., and J. L. Sarmiento, 1990: Tracer dating and ocean ventilation. *J. Geophys. Res.*, **95,** 9377–9391.

Warner, M. J., 1988: Chlorofluoromethanes F-11 and F-12: Their solubilities in water and seawater and studies of their distribution in the South Atlantic and North Pacific Oceans. Ph.D. thesis, University of California, San Diego, 124 pp.

Wunsch, C., 1988: Eclectic modelling of the North Atlantic. II Transient tracers and the ventilation of the eastern Basin thermocline. *Proc. Roy. Soc.*, **A325,** 201–233.

Young, W. R., 1984: The role of western boundary layers in gyre-scale ocean mixing. *J. Phys. Oceanogr.*, **14,** 478–483.